

## **Experimental investigations and parametric optimization during micro-EDM drilling of Ti -5.6Al-3.6V using ABC algorithm**

**DOI : 10.36909/jer.ICMET.17201**

Narender Singh\* and Pushpendra S. Bharti\*\*

\*\*USIC & T, GGS Indraprastha University, Dwarka, Delhi-110078, India

\*MSIT, C-4, Janakpuri New Delhi-110058

\* Corresponding Author: [narender\\_singh@msit.in](mailto:narender_singh@msit.in)

### **ABSTRACT**

This work presents experimental investigations and parametric optimization during micro-Electric discharge Machining (EDM) drilling of Titanium alloy Ti-5.6Al-3.6V. The experiments have been designed by response surface methodology (RSM) based central composite design (CCD) taking current, pulse-on-time and pulse-off-time as input parameters; and drill rate and tool wear ratio as performance measures. After carrying out experiments, the effect of each input parameter on performance measures has been found. In order to study the microstructure of machined surface, scanning electronic microscope (SEM) has been performed. Single objective and multi-objective optimization have been done using artificial bee colony (ABC) algorithm to find the optimal combination of input parameters for the best yield of the process. Experimental verification of the obtained results has also been performed and a difference of less than 5% has been observed between experimental values and that obtained using ABC algorithm.

**Keywords:** Ultrasonic vibration; Artificial bee colony; Tool wear ratio; Drilling rate; Central composite design; Response surface methodology.

### **INTRODUCTION**

Ti-5.6Al-3.6V is a titanium alloy that finds application in manufacturing various micro equipments and components in medical, aircraft, chemical, automotive and electronic industries. Ezugwu et al. (1997) explained that titanium has high specific strength (strength/weight ratio), greater corrosion resistance, high thermal stability and better biological

compatibility. Micro-EDM drilling is a highly suitable process for making micro-holes on this hard material. Masuzawa (2000) explained that both micro-EDM and macro EDM are working on the same thermoelectric energy principle with a little difference in spark gap control, electrode size, dielectric flow conditions and manufacturing technology. Singh et al. (2020) reported that EDM is a non-contact material removal process in which repeated spark discharges between tool and workpiece and removed conductive material through melting and vaporizing phenomena.

Li et al. (2020) investigated performance by  $\mu$ -EDM using ultrasonic circular vibration (UCV). Due to the UCV electrode, the eroded debris particles were removed effectively from the side gap simultaneously; new fresh dielectric circulated among the side gap and improved the insulation strength of the gap. Shah et al. (2021) reported the debris evacuation process under vibration and without vibration mode to find the consistency of the process. It found that vibration caused its velocity to increase by 2.2 times than no vibration condition. Li et al. (2021) found the effect of tool wear, bubbles and debris on the mechanism of discharge process. Tool wear provided a large discharge area for debris accumulation resulting in uneven material removal. The bubble diameter increased with increasing feed depth. Wasif et al. (2020) found the effect of taper-angle of specimen, current, and pulse-off-time on the responses during the wire-EDM of Ti-alloy. The taper angle is the only influencing parameter for kerf width. Feng et al. (2019) reported the effect of high spindle speed of tool electrode on performance measures like MRR, electrode wear and taper angle. The simulation was carried out to study the fluid flow field of spark gap at various rotational speeds. The results showed that higher rotational speed brought higher MRR and lower electrode wear. Huang et al. (2020) experimentally investigated the influence of capacitance, electrode number and, pulse-on-time on MRR and relative wear ratio (WR). In this method, multiple discharges were generated one by one and distributed over all electrodes uniformly. A higher value of capacitance and pulse-on-time produced higher MRR, high WR, and poor surface quality due to high discharge

energy. Singh et al. (2020) finds the integrated effect of magnetic field and ultrasonic vibration (UV) on the response variables of micro-EDM. They showed that the debris could easily be removed from the working gap even at higher depths due to combined effect. It was also observed that MRR increased while taper angle of micro-semi-circular cavity decreased. Liu et al. (2019) investigated the performance of micro-EDM with different surface treatment methods. The surface with oxidation treatment brought highest MRR than other surface treatment methods. The better performance achieved at low discharge energy. Gangil et al. (2018) applied a combined proposal of grey relational analysis (GRA) integrated with principal component analysis (PCA) for the optimization of the machining parameters. Kumar et al. (2019) used a genetic algorithm for obtaining optimal values of parameters for maximum DR and minimum electrode wear rate. Das et al. (2014) applied ABC for discovering the optimal setting for multi-responses. ABC was used for obtaining optimal values of parameters for maximum MRR and minimum surface roughness.

A lot of research work reported on EDM drilling on Titanium alloy. Though work has been reported, in literature, in micro-EDM drilling of Titanium alloys, the data is scanty in respect of micro-EDM drilling of Ti-5.6Al-3.6V. But the limited attempt was made by previous researchers to drill micro-holes on this material through RSM based experimentation. Since the combination of input parameters has direct effect of the process yield, the optimization of the input parameters has been done. For this, ABC algorithm has been employed as single objective as well as multi-objective optimization techniques.

## **EXPERIMENTATION**

The experiments have been conducted on JK machine fast drill EDM ID-25 which is three axis drilling machine. The machine consists of a co-ordinate (x-y movements) work table which is controlled manually. The tool feeding system is servo-controlled along vertical axis (z-axis). The tubular copper electrode of diameter 500  $\mu\text{m}$  has been used as tool. The Figures 1 (a) and 1 (b) show the basic diagram and real image of drill EDM set-up. Discharge current,

Pulse-on-time and pulse-off-time are taken as three important process parameters and drilling rate and tool wear ratio are chosen as the responses.

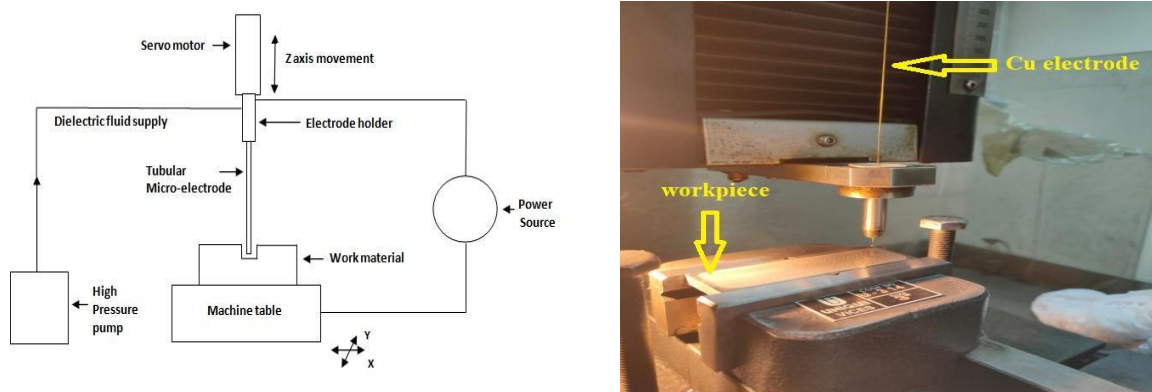


**Fig. 1(a).** EDM drill set up-block diagram      **Fig. 1(b).** EDM drill set up-real image

The specimen is rectangular in shape with dimension of 20 mm X 85 mm X 6 mm. The chemical composition and mechanical properties of specimen are given in Table 1.

**Table 1.** Chemical and Mechanical properties of Ti-5.6Al-3.6V

Work piece material	Chemical composition (wt%)	Mechanical property
Ti 5.6Al-3.6V	5.6% Al, 0.032% Fe, 3.58% V, 0.006% Ni,	Vicker hardness-345,
	0.019% Cu, 0.03% C and 90.733% Ti	Ultimate Tensile Strength-935 Mpa

**DESIGN OF EXPERIMENTS**

Experiments have been designed accordingly with CCD by taking three levels of each of the input parameters. For three input process parameters, the design needed 20 experiments with 6 factorial points, 8 axial points to form a CCD with  $\alpha=1$  and 6 centre points. The factors and their levels are shown in Table 2 with their actual values.

**Table 2.** Machining parameters and their levels

Design factors (or Input parameters)	Unit	Notation	Levels		
			Low	Middle	High
Discharge Current	Amp	$I_p$	3	5	7
Pulse-on-time	$\mu s$	$T_{on}$	30	50	70
Pulse-off-time	$\mu s$	$T_{off}$	40	60	80

The experiments have been performed according to design matrix shown in Table 3.

**Table 3.** Design matrix and experimental results

Exp. No.	I <sub>p</sub>	T <sub>on</sub>	T <sub>off</sub>	TWR	DR (mm/sec)
1	7	70	40	0.500	0.6186
2	3	30	80	0.083	0.0339
3	5	50	60	0.042	0.1116
4	5	50	60	0.167	0.1924
5	7	70	80	0.500	0.5561
6	5	50	60	0.083	0.2250
7	3	30	40	0.125	0.0271
8	7	50	60	0.583	0.6424
9	5	50	60	0.167	0.3319
10	5	70	60	0.208	0.5259
11	5	50	60	0.250	0.4345
12	3	50	60	0.083	0.0231
13	3	70	80	0.042	0.0249
14	7	30	40	0.833	0.4038
15	5	50	40	0.042	0.0475
16	5	50	80	0.167	0.2940
17	5	30	60	0.375	0.2011
18	5	50	60	0.167	0.3552
19	7	30	80	1.000	0.1332
20	3	70	40	0.042	0.0151

### **RESPONSE SURFACE METHODOLOGY**

RSM is a commonly used mathematical technique for modeling and studying the effect of different given variables over the desired response. Montgomery (2001) used this mathematical model to establish the relationship among independent variables (

$Y_1, Y_2, Y_3, \dots, Y_n$ ) and desired response ( $Y_u$ ). Usually when relationship is non-linear then a second order model is established as explained in Equation (1) as follows:

$$Y_u = \beta_0 + \sum_{i=1}^n \beta_i \cdot Y_i + \sum_{i=1}^n \beta_{ii} \cdot Y_i^2 + \sum_{i,j=1, i \neq j}^n \beta_{ij} \cdot Y_i \cdot Y_j \quad (1)$$

where,  $Y_u$  represents the desire response like DR and TWR in present research,  $Y_i$  represents input variables,  $Y_i^2$  and  $Y_i \cdot Y_j$  are squares and interaction terms of these given input variables.  $\beta_0, \beta_i, \beta_{ii}, \beta_{ij}$ , are the unknown regression coefficient..

The analysis is accomplished using design expert software. The relationship between responses and input variables in term of actual factors are given in the Equation (2) and Equation (3):

$$Y_u(DR) = -0.830436 + 0.011965 \cdot I_p - 0.023438 \cdot T_{on} + 0.042961 \cdot T_{off} + 0.002058 \cdot I_p \cdot T_{on} - 0.001092 \cdot I_p \cdot T_{off} + 0.000066 \cdot T_{on} \cdot T_{off} + 0.006215 \cdot I_p^2 + 0.000139 \cdot T_{on}^2 - 0.000343 \cdot T_{off}^2 \quad (2)$$

$$Y_u(TWR) = 0.465080 - 0.202438 \cdot I_p - 0.024411 \cdot T_{on} + 0.017562 \cdot T_{off} - 0.002214 \cdot I_p \cdot T_{on} + 0.000651 \cdot I_p \cdot T_{off} + 0.000039 \cdot T_{on} \cdot T_{off} + 0.042614 \cdot I_p^2 + 0.000322 \cdot T_{on}^2 - 0.000147 \cdot T_{off}^2 \quad (3)$$

## EXPERIMENTAL INVESTIGATION

Three process parameters are investigated for two performance measures through experimentation. In this work, DR is measured in millimeter per second and calculated as shown in the Equation (4):

$$DR = \frac{t}{T} \quad (4)$$

Where t is the thickness of specimen and T is total time taken to drill a through hole

TWR is defined as the ratio of length of tool wear to the depth of drill hole (thickness) in the specimen. It is calculated as describe in Equation (5):

$$TWR = \frac{L}{t} \quad (5)$$

The difference in tool length before and after drilling each hole is computed as length of tool wear (L). A scale is mounted along Z-axis and reference from work table measured as initial length on this scale. After drilling hole, the final length on scale is measured. Then difference between initial and final length given as length of tool wear.

### EFFECT OF PROCESS PARAMETERS ON DR AND TWR

The surface plots for DR and TWR at different parametric combination are shown in Figure 2 and Figure 3. One parameter among three process parameters has been kept constant at centre level for all these figures. It is seen that DR increases when more spark energy concentrates with high value of current and pulse-on-time.

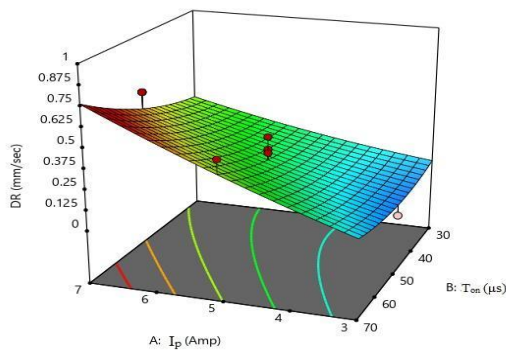


Fig. 2. a) Drill rate vs current, pulse-on-time

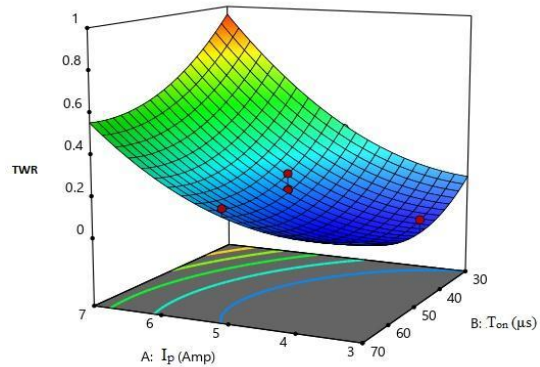


Fig. 3. a) TWR vs current, pulse-on-time

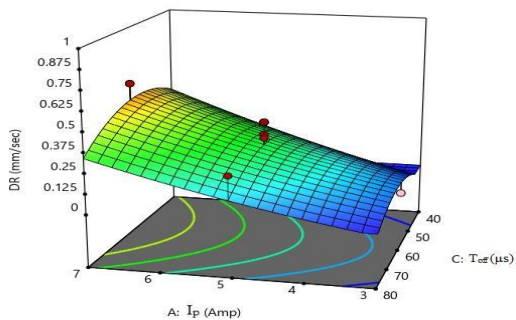


Fig. 2. b) Drill rate vs current, pulse-off-time

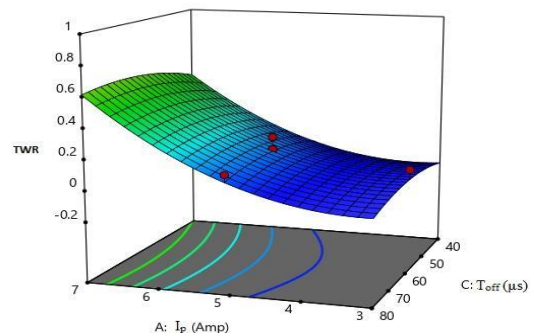
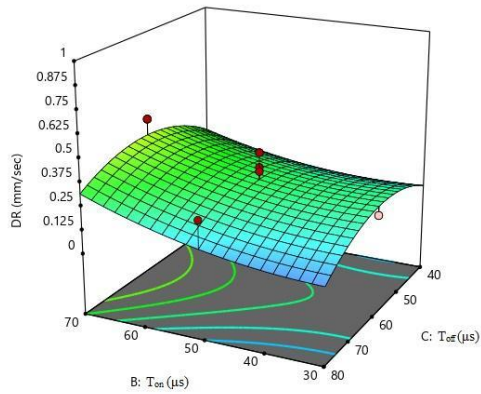
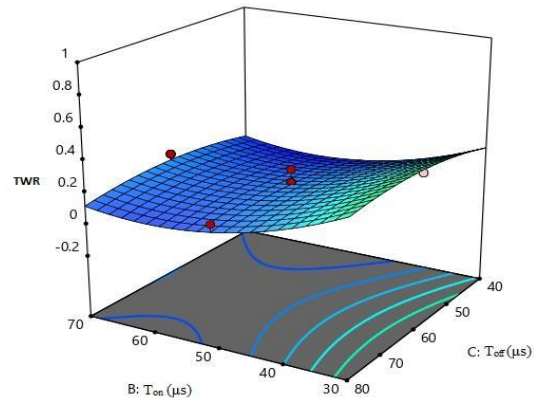


Fig. 3. b) TWR vs current, pulse-off-time



**Fig. 2. c)** Drill rate vs pulse-on-time, pulse-off-time



**Fig. 3. c)** TWR vs pulse-on-time, pulse-off-time

High current produces high spark energy that results in rapid melting; and hence drilling time reduces. As evident in Fig. 2 (b), high current with increase in pulse-off-time increases drilling rate. It may be attributed to the fact that an increment in pulse-off-time lets the debris be flushed out from the drilled hole that outcomes in a higher drilling rate. Further increase in pulse off time amounts to be higher total drilling time that ultimately results in decreased drilling rate. Fig. 2 (c) indicates that DR increases with increment in pulse-on-time and pulse-off-time up to a point and after that DR decreases with increase in these parameters.

The surface plots for tool wear ratio are shown in Fig. 3. It shows that TWR is lower when both  $I_p$  and  $T_{on}$  are decreased as shown in Fig. 3(a). With increasing  $I_p$  and  $T_{on}$ , discharge energy increases across the spark gap. The high discharge energy increases the temperature over the front face of the electrode and workpiece, resulting in increased melting and erosion of the copper electrode. Fig. 3(b) shows that high current with decrease in pulse-off-time decreases TWR. The process speed and stability depend upon  $T_{off}$ . If it is too short, it may result in unstable sparks resulting in more short-circuiting occurs, and the dielectric medium will not be deionized. Heat intensity and temperature increase rapidly so TWR increase with current. The longer pulse-off-time causes higher machining time. The optimum value of pulse-off-time provides the suitable gap in between two consecutive sparks resulting in easily

removal of debris so provide stable machining conditions and thus TWR decrease. Fig. 3(c) shows that the lowest TWR values seem at the higher  $T_{on}$  and  $T_{off}$ . If the  $T_{off}$  is insufficient against  $T_{on}$ , then it may result in irregular cycling and retraction of the advancing servo motor, decreasing the speed of the operation. Pulse-off-time should be more than deionization time to avoid sustained sparking at a single point.

### SURFACE CHARACTERIZATION

The microstructure of micro hole is characterized by melted material deposition, pockmarks and melting drops. SEM analysis is applied to analyze the surface characteristics of the machined surface. SEM images of micro-hole of Ti alloy showed poor surface texture described by the uneven fusion structure. The image showing different irregularities of micro-holes obtained at different values of current and pulse-on-time are shown in Fig. 4(a) and 4(b). High current supplied for larger duration produces high discharge energy that ultimately results in formation of deeper and larger craters near micro-drill hole.

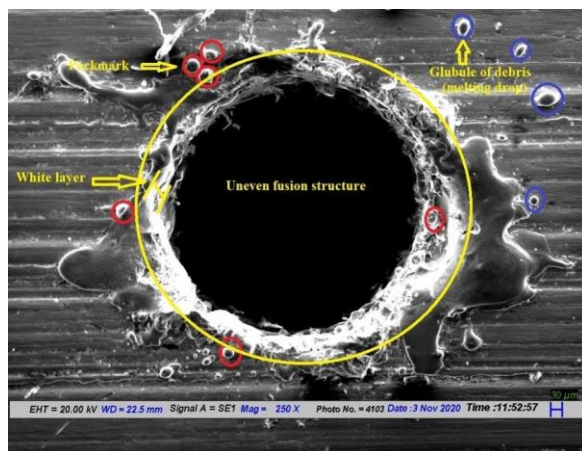


**Fig. 4. a)** SEM image of micro-hole

obtained at current ( $I_p$ ) = 7A and  $T_{on}$  = 70  $\mu$ s

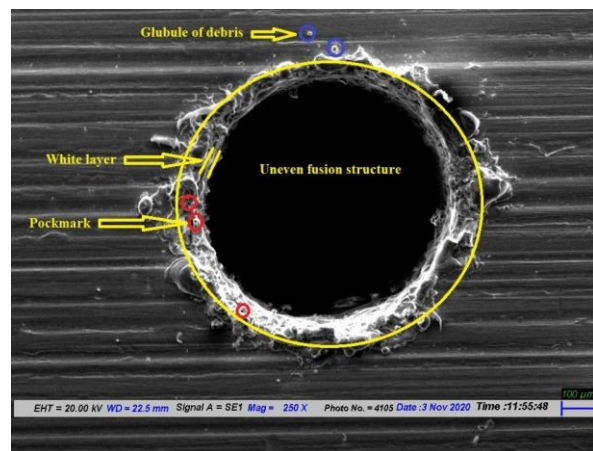


**Fig. 4. b)** SEM image of micro-hole

obtained at current ( $I_p$ ) = 5A and  $T_{on}$  = 50  $\mu$ s

The eroded material (debris) that is not flushed out by the dielectric fluid during pulse-off-time; is accumulated around micro-hole and re-solidified in the form of white layer. White layer is described by its thickness and it is very important parameter to describe morphological characteristics of micro-hole. If some crack is present near micro-hole surface, this may

propagate to the extent of white layer thickness. The SEM image showing the presence of white layer thickness onto the micro-drill hole was shown in Fig. 4(a). A comparative thin and non-uniform white layer showed on the micro-drill hole shown in Fig. 4 (b) due to the low material removal rate. Another feature of surface morphology is the availability of pockmarks in large numbers. Pockmarks are creating when entrapped gases escape during solidification. Some gases are entrapped in the mixture of wear out electrode and debris. When these entrapped gases escape from the material during solidification, pockmarks are formed. The large quantity mixture of wear-out electrode material and debris produces large number of pockmarks. High current supplied for larger duration produces high discharge energy that ultimately results in high material removal rate and high electrode wear out rate. One more important feature of surface morphology is the presence of globule of debris. As dielectric fluid cannot flush out the complete eroded particles then some particles got adhered to the machined zone result in increasing the roughness of the surface.

### **OPTIMIZATION OF PROCESS PARAMETERS**

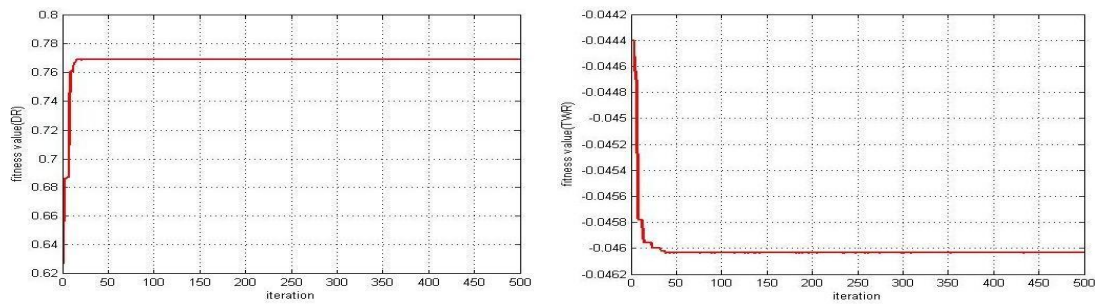
**Artificial bee colony (ABC) algorithm:** Karaboga (2005) introduced ABC inspired by the foraging behaviour of honey bees, where bees can communicate, store and share information. The foraging behavior is related to two modes; recruitment of food source and evacuation of food source. There are different types of honey bees; one is employed bees and another is unemployed bees. The employed bees explore food source (nectar position and nectar amount) and finds profitability (richness and direction from the hive) of related food source. In the hive, all employed bees accomplish waggle dance and share information about the food source. All unemployed bees also known as onlooker bees see the waggle dance and collect all the details about food source. These onlooker bees attracted towards best food source. Now onlooker bees convert to employed bees and collecting all the nectar from food source. If current food source exhausted then unemployed bees become scout bees and finding new food source. When scout bees find a new food source then these bees convert to employed bees and this cycle repeats

until best food source (optimal solution) reached. In the algorithm, both employed bee and onlooker bee are equivalent in population sizes. The Matlab code is generated for ABC algorithm using Matlab 2015.

### SINGLE OBJECTIVE OPTIMIZATION

There are two responses as described by the above equations. Each response is optimized separately using ABC algorithm. The Matlab program of ABC algorithm is run for 500 iterations and at last solution converges to optimum value as shown in Fig. 5 (a) and 5 (b).

Figure 6 displays the variation of responses (DR & TWR) with the number of iterations.



a) Single Objective optimization (DR)

b) Single Objective optimization (TWR)

**Fig. 5.** Single Objective optimization

Figures indicate that after 21 iterations solution converges to maximum DR, and after 42 iterations solution converges to minimum TWR. There is no further improvement shown in the result.

**Table 4.** Result of confirmation test for DR and TWR

Process parameters	Optimum value of DR	Optimum value of TWR	DR obtained from ABC algorithm	DR experimental value (mm/sec)	% of error of DR	TWR obtained from ABC algorithm	TWR experimental value	% of error of TWR
Current ( $I_p$ )	7.00	3.0	0.76922	0.73298	4.71	0.04603	0.043949	4.53
Pulse-on-time ( $T_{on}$ )	70.00	50.0						

Pulse-off-time ( $T_{off}$ )	60.0	40.00						
------------------------------	------	-------	--	--	--	--	--	--

The optimum value of input parameters for maximum DR and minimum TWR are shown in Table 4. The optimum values of input parameters are used to perform a confirmative experiment. The errors obtained are 4.71% for DR and 4.53% for TWR.

### MULTI-OBJECTIVE OPTIMIZATION

In multi-objective optimization technique both responses are optimized simultaneously. Rao et al. (2008) defined a new objective function for this technique as described in Equation (8).

$$Min(F) = \frac{W_1 \cdot Y_u(DR)}{TWR_{min}} - \frac{W_2 \cdot Y_u(TWR)}{DR_{max}} \tag{8}$$

Where  $Y_u(DR)$  and  $Y_u(TWR)$  are the quadric equations of drilling rate and tool wear ratio as described in Eq. (2) and Eq. (3).  $DR_{max}$  and  $TWR_{min}$  are the maximum and minimum values of the drilling rate and tool wear ratio respectively.  $W_1$  and  $W_2$  are the weightage value given to DR and TWR respectively. In this work both responses are considered for equal weight values *i.e.*  $w_1$  and  $w_2 = 0.5$ .

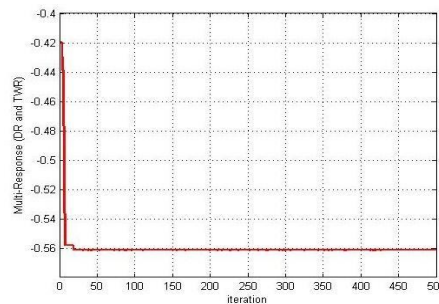


**Fig. 6.** Multi-Objective Optimization

The solution is convergence for a multi-objective response using the ABC algorithm as shown in Fig. 6. The optimum values of input parameters for maximum DR and minimum TWR are described in Table 5. The value of optimal solution (F) is -0.56146.

**Table 5.** Result of confirmation tests for DR and TWR

Process parameters	Optimum value	DR obtained from ABC algorithm	DR obtained from experimental (mm/sec)	% of error of DR	TWR obtained from ABC algorithm	TWR obtained from experimental	% of error of TWR
Current ( $I_p$ )	3.0	0.01712	0.01629	4.84	0.045677	0.04374	4.24
Pulse-on-time ( $T_{on}$ )	50.00						
Pulse-off-time ( $T_{off}$ )	80.00						

A confirmative test has been performed to verify the result of multi-objective optimization solution. The results of confirmation test for multi-objective problem are shown in Table 6. The errors are 4.84% for DR and 4.24% for TWR for multi-response optimization. The confirmative experiment results show the better compatibility between experimental and predicted value.

### CONCLUSIONS

In the present paper, DR and TWR have been investigated experimentally for EDM micro-hole drilling on Ti alloy. From this work, the following conclusions may be drawn:

- 1) DR increases when more spark energy concentrates and that happens at high value of current and pulse-on-time. Initially, DR increases with an increase in pulse-off-time because easily debris removal accelerates the drilling process. But further increase in pulse-off-time increase the total drilling time, so DR decreases.
- 2) TWR is minimum when both current and pulse-on-time decrease. Discharge energy decreases across the spark gap by reducing both current and pulse-on-time. The optimum value of pulse-off-time provides the suitable gap in between two consecutive sparks resulting in easily removal of debris so provide stable machining conditions and thus TWR decrease.
- 3) ABC algorithm applied for obtaining the optimal parametric combinations of three process parameters for optimum DR and TWR. The optimum values of input

parameters are used to perform a confirmative experiment. The errors are 4.71% for DR and 4.53% for TWR

- 4) The SEM images show larger craters and white layer thickness near micro-drill hole. The white layer thickness forms due to re-solidified of debris. The high value of current and pulse-on-time produces high discharge energy so both craters and white layer thickness increase. The Pockmarks are also shown near micro-drill hole.

#### REFERENCES

- Ezugwu, E.Q. & Wang, Z.M. 1997.** Titanium alloy and their machinability: A Review, *Journal of Material Processing Technology*, 68(3):262-274.
- Masuzawa, T. 2000.** State of the art of micro machining, *CIRP Ann. Manuf. Technol.*, 49(2):473–488.
- Singh, N. & Bharti, P.S. 2020.** A review on micro electric discharge machining of titanium alloys, *Material Today Proceeding*, 25:742–750.
- Li, Z., Tanga, J. & Bai, J. 2020.** A novel micro-EDM method to improve microhole machining performances using ultrasonic circular vibration (UCV) electrode, *Int. J. Mech. Sci.*, 175: 105574.
- Shah, M.S. & Saha, P. 2021.** Assessment of vibration-assisted micro-EDM dressing process-stability by monitoring and analyzing debris evacuation during Ti-6Al-7Nb machining, *J. Manuf. Processes*, 66:250-268.
- Li, G., Natsu, W. & Yu, Z. 2021.** Elucidation of the mechanism of the deteriorating interelectrode environment in micro EDM drilling, *Int. J. Mach. Tool Manuf.*, 167:103747.
- Wasif, M., Iqbal, S.A., Fatima, A., Yaqoob, S. & Tufail, M. 2020.** Experimental investigation for the effects of wire EDM process parameters over the tapered cross-sectional workpieces of titanium alloys (Ti6Al-4V), *Mechanical Sciences*, 11:221–232.
- Feng, G., Yang, X. & Chi, G. 2019.** Experimental and simulation study on micro hole machining in EDM with high-speed tool electrode rotation, *International Journal of Advanced Manufacturing Technology*, 101:367-375.
- Huang, R., Yi, Y., Guo, G. & Xiong, X. 2020.** Investigation of multi-electrode multi-loop with series capacitance pulse generator for EDM, *International Journal of Advanced Manufacturing Technology*, 109:143–154.
- Singh, G., Satsangi, P.S. & Prajapati, D.R. 2020.** Effect of Rotating Magnetic Field and Ultrasonic Vibration on MicroEDM Process, *Arab J. Sci. Eng. (issue 2)*.

**Liu, Q., Zhang, Q., Zhang, M., Yang, F. & Rajurkar, K.P. 2019.** Effects of surface layer of AISI 304 on micro EDM performance, *Precision Engineering*, 57:195–202.

**Gangil, M. & Pradhan, M.K. 2018.** Optimization of machining parameters of EDM for performance characteristics using RSM and GRA, *J. Mech. Eng. Biomech.*, 2(4):27-33.

**Kumar. K., Singh, V., Katyal, P. & Sharma, N. 2019.** EDM  $\mu$ -drilling in Ti-6Al-7Nb: experimental investigation and optimization using NSGA-II, *International Journal of Advanced Manufacturing Technology*, 104:2727–2738.

**Das, M.K., Kumar, K., Barman, T.K. & Sahoo, P. 2014.** Application of Artificial bee Colony Algorithm for Optimization of MRR and Surface Roughness in EDM of EN31 tool steel, *Procedia. Mater. Sci.*, 6:741–751.

**Montgomery, D.C. 2001.** *Design & Analysis of Experiments*, John Wiley, New York.

**Karaboga, D. 2005.** An Idea Based On Honey Bee Swarm For Numerical Optimization, Technical report-TR06, Erciyes University, Computer Engineering Department.

**Rao, R.V., Pawar, P.J. & Shankar, R. 2008.** Multi-objective optimization of electrochemical machining process parameters using a particle swarm optimization algorithm, *Proceeding Inst. Mech. Eng., J. Eng. Manuf.: SAGE J*, 222:949-958.